HHS Public Access

Author manuscript

Cell Rep. Author manuscript; available in PMC 2021 November 09.

Published in final edited form as:

Cell Rep. 2021 October 19; 37(3): 109870. doi:10.1016/j.celrep.2021.109870.

Loss of FBXO31-mediated degradation of DUSP6 dysregulates ERK and PI3K-AKT signaling and promotes prostate tumorigenesis

Shanshan Duan[1,2], **Loredana Moro**[1,2], **Rui Qu**[1,2], **Daniele Simoneschi**[1,2], **Hyunwoo Cho**[1,2], **Shaowen Jiang**[1,2], **Huiyong Zhao**[3], **Qing Chang**[3], **Elisa de Stanchina**[3], **Arnaldo A. Arbini**[2,4], **Michele Pagano**[1,2,5,6,*]

[1]Department of Biochemistry and Molecular Pharmacology, NYU Grossman School of Medicine, The Alexandria Center for Life Science, New York, NY 10016, USA

[2]Laura and Isaac Perlmutter Cancer Center, NYU Grossman School of Medicine, The Alexandria Center for Life Science, New York, NY 10016, USA

[3]Program in Molecular Pharmacology, Memorial Sloan Kettering Cancer Center, New York, New York 10065, USA

[4]Department of Pathology, NYU Grossman School of Medicine, The Alexandria Center for Life Science, New York, NY 10016, USA

[5]Howard Hughes Medical Institute, NYU Grossman School of Medicine, The Alexandria Center for Life Science, New York, NY 10016, USA

[6]Lead contact

SUMMARY

FBXO31 is the substrate receptor of one of many CUL1-RING ubiquitin ligase (CRL1) complexes. Here, we show that low *FBXO31* mRNA levels are associated with high pre-operative prostate-specific antigen (PSA) levels and Gleason grade in human prostate cancer. Mechanistically, the ubiquitin ligase $CRL1^{FBXO31}$ promotes the ubiquitylation-mediated degradation of DUSP6, a dual specificity phosphatase that dephosphorylates and inactivates the extracellular-signal-regulated kinase-1 and −2 (ERK1/2). Depletion of FBXO31 stabilizes DUSP6,

*Correspondence: michele.pagano@nyumc.org.

AUTHOR CONTRIBUTIONS

S.D. designed and performed most experiments and co-wrote the manuscript. R.Q. and L.M. performed some experiments and data analysis. D.S. provided critical advice. H.Z. and Q.C. performed the *in vivo* experiments. A.A.A. analyzed and scored immunohistochemistry (IHC) and H&E staining. H.C. and S.J. performed bioinformatics analyses. M.P. conceived, directed, and coordinated the study, oversaw the results, and co-wrote the manuscript. All authors discussed the results and commented on the manuscript.

DECLARATION OF INTERESTS

M.P. is a cofounder of Coho Therapeutics. He is also a consultant for, a member of the scientific advisory board of and has financial interests in Coho Therapeutics, CullGen, Kymera Therapeutics, Santi Therapeutics, and SEED Therapeutics.

SUPPLEMENTAL INFORMATION

Supplemental information can be found online at https://doi.org/10.1016/j.celrep.2021.109870.

SUPPORTING CITATIONS

The following references appear in the supplemental information: Fattore et al. (2013); Krygowska and Castellano (2018).

suppresses ERK signaling, and activates the PI3K-AKT signaling cascade. Moreover, deletion of *FBXO31* promotes tumor development in a mouse orthotopic model of prostate cancer. Treatment with BCI, a small molecule inhibitor of DUSP6, suppresses AKT activation and prevents tumor formation, suggesting that the FBXO31 tumor suppressor activity is dependent on DUSP6. Taken together, our studies highlight the relevance of the FBXO31-DUSP6 axis in the regulation of ERK- and PI3K-AKT-mediated signaling pathways, as well as its therapeutic potential in prostate cancer.

Graphical Abstract

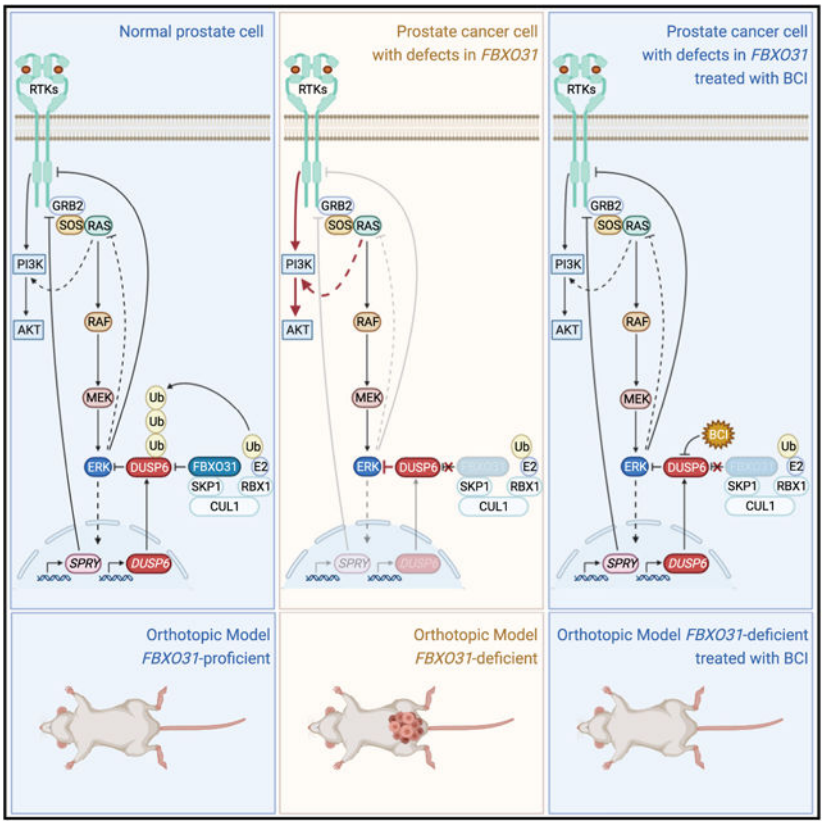

In brief

Targeted approaches for prostate cancer have recently emerged as promising therapeutic avenues. Duan et al. identify DUSP6 as the degradation target of $CRL1^{FBXO31}$, present evidence that the tumor suppressor activity of FBXO31 is dependent on DUSP6, and show that pharmacological inhibition of DUSP6 holds promise as a prostate cancer therapy.

INTRODUCTION

The ubiquitin-proteasome system (UPS) is a tightly orchestrated process of intracellular protein degradation, which plays a central role in the maintenance of cellular homeostasis (Oh et al., 2018; Pickart, 2004; Skaar and Pagano, 2009). Protein ubiquitylation occurs through a cascade of enzymatic reactions, which are catalyzed by the ubiquitin-activating

enzyme (E1), the ubiquitin-conjugating enzyme (E2), and the ubiquitin ligase (E3). E3 ubiquitin ligases selectively bind to protein targets (i.e., substrates) and contribute to their poly-ubiquitylation and consequent degradation via the 26S proteasome. However, when the regulatory mechanisms underlying the proper functioning of E3 ubiquitin ligases become aberrant, the altered protein stability of their substrates often contributes to the pathogenesis of multiple human diseases (Hoeller et al., 2006; Senft et al., 2018). With ~230 members, the cullin-RING ubiquitin ligases (CRLs) represent the largest family of E3 ubiquitin ligases in mammals. Of these, ~70 members belong to the subfamily of CUL1–RING ubiquitin ligases (CRL1s), which are also known as SKP1-CUL1-F-box protein (SCF) ubiquitin ligases, based on their ability to assemble using the small adaptor protein SKP1, the scaffold protein CUL1, and one of ~70 F-box proteins (Petroski and Deshaies, 2005; Skaar et al., 2013). In these protein complexes, F-box proteins are the variable components that selectively recruit substrates to the CRL1 core. Among the characterized mammalian F-box proteins, many are well-established tumor suppressors or oncoproteins (Skaar et al., 2014; Wang et al., 2014), indicating an important role for this protein family in cancer.

By integrating extracellular mitogen signals into intracellular signaling events, the mitogen-activated protein kinase (MAPK) pathway plays a fundamental role in cell growth and proliferation, and its deregulation in cancer has been the focus of widespread attention in the clinical setting (Simanshu et al., 2017). Upon exposure to mitogens, a series of signaling events trigger the activation of members of the Ras family of GTPases and the subsequent series of phosphorylation events that lead to the activation of the MAPK cascade (Raf-MEK1/2-ERK). ERK1/2 are the major targets of this phosphorylation cascade that conveys mitogenic signals from the plasma membrane (Lavoie et al., 2020). Activated ERK1/2 regulate several cytoplasmic and nuclear substrates, including transcription factors that control genes responsible for cell-cycle progression and proliferation (Roskoski, 2012). Importantly, a family of dual-specificity phosphatases (DUSPs; also known as MKPs for MAPK phosphatases) negatively regulates the MAPK signaling activity by dephosphorylating and inactivating ERKs (Kidger and Keyse, 2016). Several DUSPs are themselves transcriptional targets of the MAPK kinase pathway, thus acting as negative feedback regulators of the signaling cascade. Among the DUSP family members, DUSP6 is a cytoplasmic enzyme exhibiting specificity toward ERK 1/2 and represents a major regulator of these kinases (Groom et al., 1996; Muda et al., 1996). While several studies have described a tumor-suppressive function for DUSP6 (Furukawa et al., 2003; Okudela et al., 2009), growing evidence suggests that it may also play a role as an oncogene (Cui et al., 2006; Degl'Innocenti et al., 2013; Li et al., 2012; Messina et al., 2011; Shojaee et al., 2015), thus highlighting the importance for additional investigation.

Prostate cancer is the most common non-cutaneous cancer in men worldwide (https://www.wcrf.org/dietandcancer/prostate-cancer-statistics/; https://www.cancer.org/cancer/prostate-cancer/about/key-statistics.html). It is a clinically and biologically heterogeneous cancer type, and, at present, the effective clinical management of newly diagnosed patients with localized prostate cancer largely depends on tumor-related factors, including cancer extent in biopsy specimens, histological type, Gleason grade, and serum prostate-specific antigen (PSA) levels. Despite much progress that has been made on the identification of genetic drivers of prostate tumorigenesis and progression, many

molecular and actionable mechanisms still remain elusive (Shen and Abate-Shen, 2010; Wang et al., 2018).

Here, we investigated the mechanisms by which loss of *FBXO31* promotes prostate tumorigenesis and found that FBXO31 specifically interacts with DUSP6 and targets it for proteasomal degradation. Loss of FBXO31 leads to upregulation of DUSP6, which suppresses ERK signaling and releases the feedback inhibition on PI3K-AKT signaling to stimulate cell proliferation. Thus, our work provides a model for the biological function of FBXO31 in prostate tumors and demonstrates a mechanistic role for DUSP6 as a context-dependent and therapeutically actionable oncoprotein.

RESULTS

FBXO31 is a tumor suppressor in prostate epithelial cells

While investigating the methylation profile of all 69 human genes encoding F-box proteins in 15 different human cancers, we noticed that the promoter of *FBXO31* was selectively hypermethylated in prostate cancer (Moro et al., 2020; Figure S1A). Therefore, we extended this observation by interrogating databases containing information about patient-derived samples using two additional criteria: genetic alterations and alterations in mRNA levels. Our analysis showed that *FBXO31* is homozygously deleted in 9% of prostate cancer patients (Cancer Genome Atlas Research Network, 2015) (Figure S1B) and its mRNA levels are downregulated in prostate cancer specimens as compared to normal prostate samples (https://www.oncomine.org//; Figures S1C and S1D). Moreover, *FBXO31* mRNA levels negatively correlated with Gleason grade and preoperative serum PSA levels (Figures S2A and S2B), which are two commonly used prognostic factors in prostate cancer (Shen and Abate-Shen, 2010). The promoters of *FBXL4* and *FBXO16*, the other top two F-box protein-encoding genes that are homozygously deleted in prostate cancer (Figure S1B), are not among the most hypermethylated in prostate cancer (Figure S1A), and their mRNA levels are neither downregulated in prostate cancer (Figures S1C and S1D) nor correlated with preoperative PSA levels (Figures S2A and S2B). Moreover, the levels of *FBXL4* did not correlate with Gleason grade either. Another F-box protein, FBXO30, shows higher promoter methylation and low mRNA levels in prostate cancer; however, the latter did not correlate with Gleason grade and preoperative serum PSA levels (Figures S1A, S1C, S1D, S2A, and S2B).

In agreement with previous reports suggesting FBXO31 to be a tumor suppressor (Kumar et al., 2005; Tan et al., 2018), the above results suggested that loss of FBXO31 expression might play a role in the pathogenesis of prostate cancer. To test this idea, we reintroduced FBXO31 into VCAP, a prostate cancer cell line with homozygous deletion of *FBXO31* (Ghandi et al., 2019). We observed that the expression of *FBXO31* inhibited the growth of VCAP cells both in 2D and 3D cultures (Figures 1A-1C). We then knocked out *FBXO31* in RWPE1, a non-malignant prostate epithelial cell line (Figure S3; see also Figure 2B). In two different RWPE1 clones, depletion of FBXO31 promoted cell proliferation (Figure 1D). In 3D cultures, control RWPE1 cells grew spheroids with a compact morphology, whereas *FBXO31* knockout cells formed larger spheroids with irregular surfaces (Figures 1E and

1F). These data indicate that loss of FBXO31 expression in prostate epithelial cells promotes cell proliferation and adhesion-independent growth.

FBXO31 regulates ERK signaling by mediating DUSP6 degradation

To identify $CRL1^{FBXO31}$ substrates that mediate the tumor suppressor activity of FBXO31, we performed an unbiased screen that combines affinity purification of the FBXO31 complex from human cells with mass spectrometry analysis. In addition to peptides derived from the CRL1 complex subunits, CUL1 and SKP1, analysis of 2 experiments revealed 11 and 19 unique peptides, corresponding to the phosphatase DUSP6, with a 44% and 66% coverage, respectively (Figure S4A; Table S1). The interaction was confirmed by immunoprecipitation followed by immunoblotting, which showed that endogenous DUSP6 co-immunoprecipitated with FLAG-tagged FBXO31 (Figure S4B). To determine the specificity of this interaction, we used a panel of 10 F-box proteins and the 2 substrate receptors of the APC/C E3 ubiquitin ligase (CDH1 and CDC20), which often share targets with CRL1s (Skaar et al., 2009; Skaar and Pagano, 2009). We found that only FBXO31, but not any of the other substrate receptors tested, interacted with endogenous DUSP6 (Figure 2A).

The interaction of DUSP6 with FBXO31 suggested that DUSP6 could be a substrate of $CRL1^{FBXO31}$. Indeed, treatment of cells with the CRL inhibitor MLN4924 prolonged DUSP6 half-life, similar to established CRL substrates, such as p27 and cyclin D1 (Figure S4C). Knock out or knock down of *FBXO31* markedly increased the protein levels of DUSP6 and its stability in various cell lines (Figures 2B and 2C; Figure S4D). Accordingly, overexpression of wild-type FBXO31, but not FBXO31(ΔF-box), an F-box deletion mutant that cannot form a CRL1 complex, led to a reduction in DUSP6 protein levels and stability (Figure S4E). Moreover, FBXO31, but not FBXO31(ΔF-box), promoted the *in vitro* polyubiquitylation of DUSP6 (Figure 2D). Similarly, when expressed *in vivo*, wild-type FBXO31, but not FBXO31(ΔF-box), promoted the polyubiquitylation of DUSP6 (Figure S4F).

We also defined the region of human DUSP6 necessary for binding to FBXO31. We generated a series of DUSP6 deletion mutants based on its structural domains (Farooq et al., 2001) and found that amino acids 126–137, which are evolutionarily conserved in vertebrates, were required for the interaction of DUSP6 with FBXO31 (Figures S5A-S5E). Importantly, as compared to the wild-type protein, DUSP6(Δ126-137), which is unable to bind FBXO31, displayed an extended half-life (Figure S5F and S5G).

All these data strongly support the hypothesis that DUSP6 is a substrate of $CRL1^{FBXO31}$. DUSP6 is one of the major phosphatases impinging on ERK activity (Keyse, 2000). Thus, changes in DUSP6 stability are expected to have an impact on the phosphorylation and consequent activation of ERK. Indeed, we observed that, upon depletion of FBXO31 or CRL inhibition, the increase in DUSP6 levels directly correlated with a decrease in the levels of phosphorylated ERK (p-ERK) (Figures 2B and 2C; Figures S4C and S4D).

To understand the potential role of FBXO31 in growth-factor-mediated ERK signaling activation, we silenced FBXO31 expression in mouse embryonic fibroblasts (MEFs) and

examined the molecular response to epidermal growth factor (EGF) stimulation. When serum-starved MEFs were stimulated with EGF, ERK was rapidly phosphorylated and DUSP6 protein levels were decreased 15 to 30 minutes post-stimulation (Figure 2E). The levels of DUSP6 rebounded at later time points, likely due to the ERK-mediated transcriptional activation of *DUSP6* (Amit et al., 2007; Ekerot et al., 2008; Zhang et al., 2010). In contrast, there was no decrease in DUSP6 levels upon EGF stimulation of *FBXO31*-depleted MEFs, and the magnitude and duration of ERK phosphorylation were strongly reduced (Figure 2E). These results suggest that, upon stimulation with growth factors, FBXO31 is responsible for the decline in DUSP6 levels, contributing to a robust activation of ERK.

To further test the effect of FBXO31-mediated degradation of DUSP6 on ERK signaling, FBXO31 was expressed in an inducible manner, resulting in the reduction of DUSP6 levels and a corresponding increase in ERK phosphorylation (Figure S6A). Accordingly, FBXO31 induction led to the transcriptional upregulation of the so-called “ERK output,” which is defined by the mRNA levels of ERK-target genes, such as *CCND1, DUSP6, ETV5, FOSL1*, and *SPRY2* (Amit et al., 2007; Pratilas et al., 2009) (Figure S6B). Notably, upon FBXO31 expression, the protein levels of DUSP6 decreased (Figure S6A) despite the increase in DUSP6 mRNA levels (Figure S6B). Conversely, FBXO31 depletion led to the suppression of the ERK output, as shown by the reduced levels of p-ERK and the transcriptional downregulation of ERK pathway target genes in two *FBXO31* knockout clones (Figure 2B; Figure S6C). Of note, upon FBXO31 depletion, the protein levels of DUSP6 increased despite the decrease in *DUSP6* mRNA levels (Figure 2B; Figure S6C). In agreement with the results in cell systems, analysis of prostate patient samples from The Cancer Genome Atlas (TCGA) revealed a positive correlation between *FBXO31* mRNA levels and the mRNA levels of genes that are transcriptionally activated by ERK signaling (Figure 2F).

Together, these results suggest that $CRL1^{FBXO31}$ regulates the ERK pathway by promoting the degradation of DUSP6.

Loss of *FBXO31* in prostate epithelial cells enhances AKT-mediated signaling by stabilizing DUSP6

We hypothesized that the loss of *FBXO31* may facilitate prostate tumor development by regulating DUSP6 protein stability. *FBXO31*−/− RWPE1 cells proliferated faster than parental cells (Figures 1D and 3A). To assess if the increase in cell proliferation due to *FBXO31* loss was dependent on DUSP6 stabilization, we utilized 2-benzylidene-3-(cyclohexylamino)-1-Indanone hydrochloride (BCI), a selective small-molecule inhibitor of DUSP6 (Korotchenko et al., 2014; Molina et al., 2009; Shojaee et al., 2015; Unni et al., 2018). Inhibition of DUSP6 efficiently abolished the growth advantage induced by the deletion of *FBXO31* (Figure 3A). Furthermore, *FBXO31* knockout cells were more sensitive to DUSP6 inhibition than parental cells in both 2D and 3D cultures (Figures S7A-S7D). These data support the hypothesis that DUSP6 accumulation is a major mediator of cell proliferation induced by *FBXO31* loss.

The above results indicated that *FBXO31* loss provides a gain-of-function to prostate cancer cells by inhibiting the ERK pathway, which may appear as counterintuitive at first. While

analyzing the TCGA database, we noticed an intriguing correlation between *FBXO31* loss and the genetic alterations of the PTEN-PI3K-AKT signaling pathway components, which are frequently deregulated in prostate tumors (Cancer Genome Atlas Research Network, 2015; Manning and Toker, 2017; Taylor et al., 2010). We observed that the large majority of *PTEN* deep deletions, as well as amplifications and activating mutations in *PIK3CA, AKT1*, and *AKT2*, were mutually exclusive with both *FBXO31* deletions and *DUSP6* amplifications (Figure S8A). Previous studies have demonstrated the existence of an ERK-mediated negative feedback signal on both RAS/MEK/ERK and RAS/PI3K/AKT pathways (Castellano and Downward, 2011; Kodaki et al., 1994; Lake et al., 2016; Lito et al., 2013; Manning and Toker, 2017; Mendoza et al., 2011; Rodriguez-Viciana et al., 1994; Turke et al., 2012). Since FBXO31 loss leads to ERK inhibition, we also assessed its impact on AKT activity and found that the deletion of *FBXO31* increases the levels of phosphorylated AKT (p-AKT) (Figure 2B). Reintroduction of FBXO31 into VCAP cells led to a decrease in the levels of DUSP6, an increase in the levels of p-ERK, and a concomitant decrease in p-AKT levels (Figure 3B). Accordingly, treatment of VCAP parental cells with an ERK inhibitor (i.e., SCH772984) led to a rapid increase in p-AKT levels (Figure S8B). Moreover, treatment of RWPE1 cells with the DUSP6 inhibitor BCI led to elevated p-ERK levels and a decrease in the levels of both p-MEK and p-AKT (Figure 3C). This observation further confirms that targeting DUSP6, either by mediating its protein degradation or inhibiting its phosphatase activity, affects AKT signaling.

Since (1) FBXO31 silencing affects the ERK phosphorylation response to EGF stimulation (Figure 2E) and (2) EGF stimulates the proliferation of prostate epithelial cells (Bello et al., 1997), we measured the molecular responses to EGF deprivation in RWPE1 cells, which are routinely cultured in the presence of EGF-containing medium. Whereas EGF withdrawal caused a decrease in both ERK and AKT signaling in parental cells, *FBXO31* knockout RWPE1 cells showed a more rapid decrease in the levels of p-ERK, likely due to the sustained levels of DUSP6 (Figure 3D). In contrast, the decline of p-AKT levels was significantly delayed in *FBXO31*$^{-/-}$ RWPE1 cells. Accordingly, the decrease in the phosphorylated forms of S6K and 4E-BP, two downstream effectors of the AKT signaling (Manning and Cantley, 2007), was also delayed in *FBXO31* knockout RWPE1 cells. Moreover, in response to EGF withdrawal, RAS activity (detected by a RAS-GTP pull-down assay) decreased in parental cells but not significantly in *FBXO31* knockout RWPE1 cells (Figure 3E). Notably, treatment with the DUSP6 inhibitor BCI rescued the effect induced by the loss of *FBXO31*. Finally, *FBXO31* knockout RWPE1 cells continued to grow for up to 4 days upon EGF deprivation whereas parental cells did not (Figure 3F), indicating that their ability to proliferate was growth-factor-independent.

Because of the increased AKT activation in *FBXO31* knockout cells, we used the AKT inhibitor MK2206 to assess its effect on cell proliferation. We found that RWPE1 *FBXO31* knockout cells were more sensitive to MK2206 treatment than parental RWPE1 cells (Figure S8C). Moreover, AKT inhibition abolished the growth advantage induced by FBXO31 depletion (Figure S8D).

All these observations indicate that DUSP6 stabilization limits ERK activity, thereby relieving its established negative feedback activity toward RAS, which, in turn, impinges on the PI3K-AKT signaling.

Deletion of *FBXO31* promotes prostate tumor formation and sensitizes tumors to DUSP6 inhibition

Next, we asked whether our observations were also valid *in vivo* using an orthotopic model of prostate cancer. RWPE1 are non-malignant prostate epithelial cells that require androgen for their growth (Bello et al., 1997). Consistent with previous reports (Bello et al., 1997; Webber et al., 2001), orthotopic injection of RWPE1 cells did not form tumors either in the presence or absence of testosterone (Figure 4A). In contrast, injection of two different *FBXO31* knockout RWPE1 clones into the prostate of testosterone-supplemented immunodeficient mice resulted in the formation of tumors (Figure 4A). Importantly, administration of the DUSP6 inhibitor BCI fully reverted the oncogenic effect of *FBXO31* loss (Figure 4A). We also performed hematoxylin and eosin (H&E) staining of paraffin sections from the dissected tissues. As compared to prostates injected with parental cells, xenografts from mice injected with *FBXO31* knockout RWPE1 cells in the presence of testosterone exhibited features of a high histologic tumor grade (Figure 4B). Moreover, immunohistochemical analysis showed decreased p-ERK expression and high levels of p-AKT in *FBXO31* knockout xenografts (Figure 4B-C), consistent with our data in cell systems. These phenotypes could be reversed by BCI treatment, suggesting that the oncogenic effect of *FBXO31* loss is mainly due to the stabilization of DUSP6.

Taken together, these data indicate that genetic loss of *FBXO31* in prostate epithelial cells inhibits ERK activity and induces AKT activation, promoting prostate tumorigenesis.

DISCUSSION

Here, we report a tumor suppressor role for FBXO31 in prostate cancer. *FBXO31* mRNA levels are downregulated in prostate cancer patients, and these low levels correlate with high preoperative PSA levels and Gleason grade, suggesting that loss of FBXO31 may be clinically relevant in the pathogenesis of prostate cancer. Mechanistically, we found that FBXO31 functions by targeting the phosphatase DUSP6 for ubiquitin- and proteasome-mediated degradation. DUSP6 is a key regulator of ERK activity and, at the same time, a transcriptional target of the ERK signaling pathway, thereby acting as a negative feedback regulator. We found that the FBXO31-mediated degradation of DUSP6 affects the ERK signaling cascade in response to EGF stimulation, and we propose that the degradation of DUSP6 plays a key role in regulating the extension and duration of ERK activation by mitogens. This could be crucial for determining cell fate since the kinetics of ERK activity has been proven to be important for the regulation of cell proliferation and differentiation (Marshall, 1995; von Kriegsheim et al., 2009).

FBXO31 loss further attenuates ERK activity in response to EGF withdrawal but potentiates AKT activity and promotes cell proliferation even in the absence of EGF. We noticed that in prostate cancer, *FBXO31* deletions, *DUSP6* amplifications, and genetic alterations in the PTEN-PI3K-AKT pathway are mutually exclusively distributed across tumor genomes.

AKT signaling is one of the most commonly deregulated pathways in prostate cancer, and, in fact, prostate cancer cells are often addicted to AKT activity (Shen and Abate-Shen, 2010; Wang et al., 2018). ERK and AKT signaling pathways are known to crosstalk, and a negative feedback from ERK to AKT has been well established (Castellano and Downward, 2011; Mendoza et al., 2011; Turke et al., 2012; Yu et al., 2002). Clinical evidence also showed a negative correlation between ERK and AKT activity in prostate cancer (Malik et al., 2002; Paweletz et al., 2001). For example, analysis of p-AKT and p-ERK levels in prostate cancer samples revealed that the p-AKT staining intensity is significantly greater in Gleason grades 8 to 10 as compared to lower grades and prostatic intraepithelial neoplasia (Malik et al., 2002). The staining intensity for p-ERK, on the other hand, declines with disease progression, reaching its lowest level of expression in high Gleason grades 8 to 10 (Malik et al., 2002). These observations suggest that advanced disease is accompanied by hyperactivation of AKT and lowERK activity. We showed that in non-malignant prostate epithelial cells, loss of FBXO31 leads to DUSP6 accumulation, lower ERK activity, activation of PI3K-AKT signaling, and enhanced cell proliferation (see model in Figure S8E). We also observed that overexpression of FBXO31 leads to ERK activation and a parallel inhibition of AKT signaling, which could be responsible for growth inhibition. These data are in agreement with other studies proposing *DUSP6* as a context-dependent oncogene (Kidger and Keyse, 2016) and further extend these observations at the mechanistic level by indicating that its oncogenic role in prostate cancer development is dependent on the ERK-mediated negative feedback on PI3K-AKT signaling. Obviously, we cannot exclude that the oncogenic role of DUSP6 may impinge on additional pathways.

Cyclin D1, a major driver of cell proliferation and growth, has been previously identified to be a substrate of FBXO31 (Santra et al., 2009). While this observation could have possibly corroborated the function of FBXO31 as a negative regulator of cell proliferation and a tumor suppressor, emerging evidence has revealed that cyclin D1 turnover is unaffected by FBXO31 (Kanie et al., 2012). Indeed, two recent studies have identified the ubiquitin ligase ($CRL4^{AMBRA1}$) targeting cyclin D1 for degradation and, at the same time, disproved a role for $CRL1^{FBXO31}$ in the regulation of cyclin D1 (Chaikovsky et al., 2021; Simoneschi et al., 2021). Other FBXO31 substrates have been previously reported, including MDM2 (Malonia et al., 2015), CDT1 (Johansson et al., 2014), and FOXM1 (Jeffery et al., 2017). We could not detect the interaction between FBXO31 and MDM2 in our experimental settings. Since the focus of this study is the role of FBXO31 in regulating the ERK signaling in response to extracellular stimulation, we did not evaluate FOXM1 and CDT1, which are substrates whose functions are later in the cell cycle.

Emerging data suggest that inhibiting DUSP6 could be a potential therapeutic strategy in certain types of tumors, such as glioblastoma, papillary thyroid carcinoma, and leukemia (Degl'Innocenti et al., 2013; Kaltenmeier et al., 2017; Messina et al., 2011; Shojaee et al., 2015). The DUSP6 inhibitor BCI is under clinical investigation as an anticancer therapeutics for patients with leukemia and solid tumors (Ramkissoon et al., 2019; Shojaee et al., 2015; Unni et al., 2018; Wu et al., 2018). BCI is an allosteric inhibitor of DUSP6 that binds near the active site of the phosphatase and inhibits its catalytic activation. We observed that *FBXO31*-deficient RWPE1 cells were more sensitive to the growth inhibitory effects of BCI than parental cells, and we recapitulated these findings in an *in vivo* orthotopic mouse model

of prostate cancer. Therefore, our studies suggest that the "addiction" of *FBXO31*-deficient prostate cancer cells to DUSP6 represents a vulnerability that can be clinically exploited.

STAR★METHODS

RESOURCE AVAILABILITY

Lead contact—Further information and requests for resources and reagents may be directed to and will be fulfilled by the Lead Contact, Michele Pagano (michele.pagano@nyumc.org).

Materials availability—Plasmids and other reagents generated in this study are available by contacting the Lead Contact, Michele Pagano (michele.pagano@nyumc.org).

Data and code availability

- Original western blot images have been deposited at Mendeley and are publicly available as of the date of publication. The DOI is listed in the key resources table. All other data reported in this paper will be shared by the Lead Contact upon request.
- This paper does not report original code.
- Additional information required to reanalyze the data reported in this paper is available from the Lead Contact upon request.

EXPERIMENTAL MODEL AND SUBJECT DETAILS

Cell culture procedures—HEK293T (female), 293H (unknown sex), VCAP (male), A375 (female) and SK-MEL-28 (male) cell lines and MEFs (unknown sex) were cultured in DMEM medium supplemented with 10% fetal bovine serum (FBS) (Corning Life Sciences) and 1% penicillin/streptomycin/L-glutamine (Corning Life Sciences). For cells stably infected with doxycycline-inducible vectors, cells were propagated in media supplemented with 10% Tet system-approved FBS (Takara/Clontech Laboratories). RWPE1 (male) cells were cultured with the Keratinocyte Serum Free Medium (K-SFM) supplemented with bovine pituitary extract (BPE) and human recombinant epidermal growth factor (EGF) obtained from Thermo Fisher Scientific (Cat. No. 17005-042). Cells were periodically screened for Mycoplasma contamination. No cell lines used in this study were found in the database of commonly misidentified cell lines that is maintained by ICLAC and NCBI Biosample. Specific details about cell lines used are provided in the Key Resource Table.

Mice model, histological and IHC staining—NSG male mice, 6-8 weeks old were obtained from the Jackson Laboratory and maintained in compliance with Institutional Animal Care and Use Committee (IACUC) guidelines. Mice were injected with $0.5x10^6$ cells orthotopically in the prostate (n = 5 mice/group). Where indicated, testosterone pellets (12.5 mg, 90 days release) were implanted at time of cell injections. Mice were administered with DUSP6 inhibitor BCI (10mg/kg) or PBS (as vehicle) via intraperitoneal injection for five consecutive days per week, until experimental endpoint. Bioimaging was performed at different time points/once per week starting one week post cell implantation using an

in vivo IVIS (100 bioluminescence/optical imaging system (xenogen)). All studies were performed in compliance with institutional guidelines under an IACUC-approved protocol. Tumor specimens were fixed in 10% neutral-buffered formalin and embedded in paraffin. Serial sections were cut on a microtome and mounted on glass slides. Histopathological examination and IHC were performed as previously described (Lignitto et al., 2019; Moro et al., 2020). All tumor burden and IHC analyses were done in a blinded fashion, in which the pathologist was unaware of the samples' genotype. Pictures were obtained using a digital whole-slide scanner (Leica, SCN400F) and Slidepath software version 4.0.8.

METHOD DETAILS

Reagents and biochemical methods—Immunoprecipitation, immunoblotting experiments and Mass Spectrometry analysis were performed as previously described (Lignitto et al., 2019). Briefly, whole-cell lysates were generated by lysing cells in 50 mM Tris pH 7.5, 150 mM NaCl, 0.5% NP40, 1 mM EDTA, 10% glycerol, protease inhibitor mix (Roche) and phosphatase inhibitor cocktail (Sigma). Total protein amount was measured using a Spectramax spectrophotometer (Molecular Devices, Sunnyvale, CA, USA). Doxycycline (Sigma-Aldrich) was used at 0.1 μg/mL, Cycloheximide (Sigma-Aldrich) was used at 50 μg/mL, MLN4924 (Active Biochem) was used at 2 μM and MG132 (Peptides International) was used at 10 μM. (E/Z)-BCI hydrochloride, PhosSTOP phosphatase inhibitor cocktail tablets were purchased from Sigma-Aldrich. Matrigel Matrix Phenol Red-Free was purchased from Corning. Recombinant Human EGF Protein was obtained from R&D Systems. Purified E1, E2s and ubiquitin were purchased from Boston Biochem (now R&D Systems).

Gene silencing—ON-TARGETplus Human FBXO31 siRNAs (Dharmacon, LQ-016541-00-0005) were transfected into different cell lines using RNAi Max (Thermo Fisher Scientific). ON-TARGETplus non-targeting siRNA #1 (GE Healthcare, catalog no. D-001810-01) served as a negative control. shRNA against *FBXO31* in MEFs was a gift from Dr. K. I. Nakayama's lab (Kanie et al., 2012).

CRISPR-Cas9 mediated gene knockout—Human *FBXO31* knockout cell lines were generated according to previously published protocol (Ran et al., 2013). Briefly, optimal gRNA target sequences were designed using the Benchling CRISPR Genome Engineering tool. gRNA target sequences were cloned into pSpCas9(BB)-2A-GFP (PX458) plasmid, a gift from F. Zhang (Addgene plasmid no. 48138). The gRNA-containing PX458 were transiently transfected into cells and single clones were isolated into 96 well plates by sorting GFP positive cells using FACS (SY3200 highly automated parallel sorting cell sorter). About two weeks later, cell clones were analyzed for genotyping. Genomic DNA was collected using QuickExtract (Epicenter). Genotyping PCRs were performed with MyTaq HS Red Mix (Bioline) using primers surrounding the genomic target site. The resulting PCR products were purified and sequenced to determine the presence of an indel event. To further validate the mutational status of candidate clones, the PCR products were subjected to TOPO-TA Cloning (Invitrogen), and sequenced to distinguish the amplified products of distinct alleles. Clones positive to insertion or deletion events were validated also by western blot. The oligos sequences used for CRISPR gDNA are:

hFBXO31_gRNA#1 forward: 5′-caccgGCGACGGGCCCACGCCGCAA-3′

hFBXO31_gRNA#1 reverse: 5′-aaacTTGCGGCGTGGGCCCGTCGCc-3′

hFBXO31_gRNA#2 forward: 5′-caccgGGCGCCGACATCCGCGCGAC-3′

hFBXO31_gRNA#2 reverse: 5′-aaacGTCGCGCGGATGTCGGCGCCc-3′

For CRISPR genotyping, sequencing genomic DNA was performed using the following primers (forward) 5′-GTTTTGCACTCGGC ATCAC-3′ and (reverse) 5′-CCCTAACCGCCTCAAATACC-3′.

Quantitative real-time PCR—Total RNA from cells was extracted using RNeasy isolation kit from QIAGEN (Valencia, CA). cDNA was generated using RNA to cDNA EcoDry™ Premix (Oligo dT) kit (Takara Bio USA, Inc). Applied Biosystems Taqman probes (Thermo Fisher Scientific) were used to determine the amount of mRNA expression for *FBXO31, DUSP6, CCND1, SPRY2, SPRY4, ETV1* or *ETV5* relative to the endogenous control gene (GAPDH).

Cell viability/proliferation assays in 2D and 3D culture—For the growth assays, cells were plated in 96-well plates at a density of 5000-8000 cells/well. Cells were lysed on the indicated days with CellTiter-Glo® Luminescent Cell Viability Assay reagent (Promega, Madison, WI, USA) and luminescence was read using Tecan infinite M200 Pro plate reader. For viability experiments, cells were seeded in 96-well plates and exposed to the DUSP6 inhibitor (BCI) at various concentrations on the following day. At 72 h after drug addition, CellTiter-Glo reagent was added and luminescence was measured. For each condition, 8 replicates of each concentration were measured. IC_{50} values were calculated using GraphPad Prism 8. Three-dimensional culture was performed following the protocol (Lee et al., 2007). Cells were seeded in 96 well plate (Corning Costar #3603) on a layer of Matrigel. For BCI treatment, different concentrations of the inhibitor were added the next day. After 10-14 days, cells were measured by the CellTiter-Glo® 3D Cell Viability Assay (Promega, Madison, WI, USA) according to the manufacturer's instructions. Data were collected from 3 independent experiments.

***In vivo* and *in vitro* ubiquitylation assay—**For detection of ubiquitinated proteins *in vivo*, cells were transfected with expression vectors for His-Myc-ubiquitin and the indicated proteins. Cells were treated with 10 μM MG132 for 4 h to block proteasome degradation before harvest. The cell lysates were boiled, sonicated, and diluted 10 times with Tris-buffered saline without SDS. The solution was then subjected to immunoprecipitation with anti-HA antibody and immunoblotting with the indicated antibodies. *In vitro* ubiquitylation was performed as previously described (Duan et al., 2012).

Human clinical data analysis—Genomic data, gene expression data and clinical data for subjects with prostate adenocarcinoma were collected from cBioPortal (Cancer Genome Atlas Research Network, 2015; Gao et al., 2013) The promoter methylation analysis was performed as previously described (Moro et al., 2020). The human pan-cancer methylation database, MethHC (Huang et al., 2015), was used to calculate the average beta value in

tumor samples and matched normal samples for different genes. The methylation scores were obtained by the ratio between the median beta value of tumor samples and the median beta value of the corresponding matched normal samples. F-box genes were then ranked by the methylation scores. For the gene expression analysis, the gene expression Z score of *FBXO31* gene from RNA-seq was used as a classifier in defining the subgroups. The top 25% and bottom 25% of patients were selected.

Active RAS assay—Cells were cultured in 10-cm plates until 70%–80% confluent. GTP-bound RAS was quantified using RAF1 Ras-binding domain (RBD) pull-down from Detection Kit (Thermo Scientific, no. 16117), as per the manufacturer.

QUANTIFICATION AND STATISTICAL ANALYSIS

Data were analyzed using GraphPad Prism 8. Unless otherwise stated in the figure legends, data are representative of at least three independent experiments. Statistical significance was assessed using unpaired two-tailed Student's t tests, one-way ANOVA multiple-comparison test or two-tailed log-rank tests. P values are provided in the figures or in the figure legends. $p < 0.05$ was considered to be statistically significant.

Supplementary Material

Refer to Web version on PubMed Central for supplementary material.

ACKNOWLEDGMENTS

The authors thank Dr. Keiichi I. Nakayama and Dr. Neal Rosen for reagents, Dr. Julia Pagan and Na Na for their help, the NYU Center for Biospecimen Research and Development (CBRD), and the NYU Langone's Proteomics Laboratory. M.P. is an investigator with the Howard Hughes Medical Institute. M.P. is grateful to T.M. Thor and T.B. Balduur for continuous support. This work was funded by grants from the National Institute of Health (R01-CA76584 and R35-GM136250) to M.P. S.D. was supported in part by the National Institute of Health Training Program in Molecular Oncology and Tumor Immunology (2T32CA009161). L.M. is on sabbatical from the Institute of Biomembranes, Bioenergetics and Molecular Biotechnologies, National Research Council, 70126 Bari, Italy.

REFERENCES

Amit I, Citri A, Shay T, Lu Y, Katz M, Zhang F, Tarcic G, Siwak D, Lahad J, Jacob-Hirsch J, et al. (2007). A module of negative feedback regulators defines growth factor signaling. Nat. Genet 39, 503–512. [PubMed: 17322878]

Bello D, Webber MM, Kleinman HK, Wartinger DD, and Rhim JS (1997). Androgen responsive adult human prostatic epithelial cell lines immortalized by human papillomavirus 18. Carcinogenesis 18, 1215–1223. [PubMed: 9214605]

Cancer Genome Atlas Research Network (2015). The Molecular Taxonomy of Primary Prostate Cancer. Cell 163, 1011–1025. [PubMed: 26544944]

Castellano E, and Downward J (2011). RAS Interaction with PI3K: More Than Just Another Effector Pathway. Genes Cancer 2, 261–274. [PubMed: 21779497]

Chaikovsky AC, Li C, Jeng EE, Loebell S, Lee MC, Murray CW, Cheng R, Demeter J, Swaney DL, Chen SH, et al. (2021). The AMBRA1 E3 ligase adaptor regulates the stability of cyclin D. Nature 592, 794–798. [PubMed: 33854239]

Cui Y, Parra I, Zhang M, Hilsenbeck SG, Tsimelzon A, Furukawa T, Horii A, Zhang ZY, Nicholson RI, and Fuqua SA (2006). Elevated expression of mitogen-activated protein kinase phosphatase 3 in breast tumors: a mechanism of tamoxifen resistance. Cancer Res. 66, 5950–5959. [PubMed: 16740736]

Degl'Innocenti D, Romeo P, Tarantino E, Sensi M, Cassinelli G, Catalano V, Lanzi C, Perrone F, Pilotti S, Seregni E, et al. (2013). DUSP6/MKP3 is overexpressed in papillary and poorly differentiated thyroid carcinoma and contributes to neoplastic properties of thyroid cancer cells. Endocr. Relat. Cancer 20, 23–37. [PubMed: 23132790]

Duan S, Cermak L, Pagan JK, Rossi M, Martinengo C, di Celle PF, Chapuy B, Shipp M, Chiarle R, and Pagano M (2012). FBXO11 targets BCL6 for degradation and is inactivated in diffuse large B-cell lymphomas. Nature 481, 90–93. [PubMed: 22113614]

Ekerot M, Stavridis MP, Delavaine L, Mitchell MP, Staples C, Owens DM, Keenan ID, Dickinson RJ, Storey KG, and Keyse SM (2008). Negative-feedback regulation of FGF signalling by DUSP6/MKP-3 is driven by ERK1/2 and mediated by Ets factor binding to a conserved site within the DUSP6/MKP-3 gene promoter. Biochem. J 412, 287–298. [PubMed: 18321244]

Farooq A, Chaturvedi G, Mujtaba S, Plotnikova O, Zeng L, Dhalluin C, Ashton R, and Zhou MM (2001). Solution structure of ERK2 binding domain of MAPK phosphatase MKP-3: structural insights into MKP-3 activation by ERK2. Mol. Cell 7, 387–399. [PubMed: 11239467]

Fattore L, Marra E, Pisanu ME, Noto A, de Vitis C, Belleudi F, Aurisicchio L, Mancini R, Torrisi MR, Ascierto PA, and Ciliberto G (2013). Activation of an early feedback survival loop involving phospho-ErbB3 is a general response of melanoma cells to RAF/MEK inhibition and is abrogated by anti-ErbB3 antibodies. J. Transl. Med 11, 180. [PubMed: 23890105]

Furukawa T, Sunamura M, Motoi F, Matsuno S, and Horii A (2003). Potential tumor suppressive pathway involving DUSP6/MKP-3 in pancreatic cancer. Am. J. Pathol 162, 1807–1815. [PubMed: 12759238]

Gao J, Aksoy BA, Dogrusoz U, Dresdner G, Gross B, Sumer SO, Sun Y, Jacobsen A, Sinha R, Larsson E, et al. (2013). Integrative analysis of complex cancer genomics and clinical profiles using the cBioPortal. Sci. Signal 6, pl1. [PubMed: 23550210]

Ghandi M, Huang FW, Jané-Valbuena J, Kryukov GV, Lo CC, McDonald ER 3rd, Barretina J, Gelfand ET, Bielski CM, Li H, et al. (2019). Next-generation characterization of the Cancer Cell Line Encyclopedia. Nature 569, 503–508. [PubMed: 31068700]

Groom LA, Sneddon AA, Alessi DR, Dowd S, and Keyse SM (1996). Differential regulation of the MAP, SAP and RK/p38 kinases by Pyst1, a novel cytosolic dual-specificity phosphatase. EMBO J. 15, 3621–3632. [PubMed: 8670865]

Hoeller D, Hecker CM, and Dikic I (2006). Ubiquitin and ubiquitin-like proteins in cancer pathogenesis. Nat. Rev. Cancer 6, 776–788. [PubMed: 16990855]

Huang WY, Hsu SD, Huang HY, Sun YM, Chou CH, Weng SL, and Huang HD (2015). MethHC: a database of DNA methylation and gene expression in human cancer. Nucleic Acids Res. 43, D856–D861. [PubMed: 25398901]

Jeffery JM, Kalimutho M, Johansson P, Cardenas DG, Kumar R, and Khanna KK (2017). FBXO31 protects against genomic instability by capping FOXM1 levels at the G2/M transition. Oncogene 36, 1012–1022. [PubMed: 27568981]

Johansson P, Jeffery J, Al-Ejeh F, Schulz RB, Callen DF, Kumar R, and Khanna KK (2014). SCF-FBXO31 E3 ligase targets DNA replication factor Cdt1 for proteolysis in the G2 phase of cell cycle to prevent re-replication. J. Biol. Chem 289, 18514–18525. [PubMed: 24828503]

Kaltenmeier CT, Vollmer LL, Vernetti LA, Caprio L, Davis K, Korotchenko VN, Day BW, Tsang M, Hulkower KI, Lotze MT, and Vogt A (2017). A Tumor Cell-Selective Inhibitor of Mitogen-Activated Protein Kinase Phosphatases Sensitizes Breast Cancer Cells to Lymphokine-Activated Killer Cell Activity. J. Pharmacol. Exp. Ther 361, 39–50. [PubMed: 28154014]

Kanie T, Onoyama I, Matsumoto A, Yamada M, Nakatsumi H, Tateishi Y , Yamamura S, Tsunematsu R, Matsumoto M, and Nakayama KI (2012). Genetic reevaluation of the role of F-box proteins in cyclin D1 degradation. Mol. Cell. Biol 32, 590–605. [PubMed: 22124152]

Keyse SM (2000). Protein phosphatases and the regulation of mitogen-activated protein kinase signalling. Curr. Opin. Cell Biol 12, 186–192. [PubMed: 10712927]

Kidger AM, and Keyse SM (2016). The regulation of oncogenic Ras/ERK signalling by dual-specificity mitogen activated protein kinase phosphatases (MKPs). Semin. Cell Dev. Biol 50, 125–132. [PubMed: 26791049]

Kodaki T, Woscholski R, Hallberg B, Rodriguez-Viciana P, Downward J, and Parker PJ (1994). The activation of phosphatidylinositol 3-kinase by Ras. Curr. Biol 4, 798–806. [PubMed: 7820549]

Korotchenko VN, Saydmohammed M, Vollmer LL, Bakan A, Sheetz K, Debiec KT, Greene KA, Agliori CS, Bahar I, Day BW, et al. (2014). In vivo structure-activity relationship studies support allosteric targeting of a dual specificity phosphatase. ChemBioChem 15, 1436–1445. [PubMed: 24909879]

Krygowska AA, and Castellano E (2018). PI3K: A Crucial Piece in the RAS Signaling Puzzle. Cold Spring Harb. Perspect. Med 8, a031450. [PubMed: 28847905]

Kumar R, Neilsen PM, Crawford J, McKirdy R, Lee J, Powell JA, Saif Z, Martin JM, Lombaerts M, Cornelisse CJ, et al. (2005). FBXO31 is the chromosome 16q24.3 senescence gene, a candidate breast tumor suppressor, and a component of an SCF complex. Cancer Res. 65, 11304–11313. [PubMed: 16357137]

Lake D, Corrêa SA, and Müller J (2016). Negative feedback regulation of the ERK1/2 MAPK pathway. Cell. Mol. Life Sci 73, 4397–4413. [PubMed: 27342992]

Lavoie H, Gagnon J, and Therrien M (2020). ERK signalling: a master regulator of cell behaviour, life and fate. Nat. Rev. Mol. Cell Biol 21, 607–632. [PubMed: 32576977]

Lee GY, Kenny PA, Lee EH, and Bissell MJ (2007). Three-dimensional culture models of normal and malignant breast epithelial cells. Nat. Methods 4, 359–365. [PubMed: 17396127]

Li W, Song L, Ritchie AM, and Melton DW (2012). Increased levels of DUSP6 phosphatase stimulate tumourigenesis in a molecularly distinct melanoma subtype. Pigment Cell Melanoma Res. 25, 188–199. [PubMed: 22171919]

Lignitto L, LeBoeuf SE, Homer H, Jiang S, Askenazi M, Karakousi TR, Pass HI, Bhutkar AJ, Tsirigos A, Ueberheide B, et al. (2019). Nrf2 Activation Promotes Lung Cancer Metastasis by Inhibiting the Degradation of Bach1. Cell 178, 316–329.e18. [PubMed: 31257023]

Lito P, Rosen N, and Solit DB (2013). Tumor adaptation and resistance to RAF inhibitors. Nat. Med 19, 1401–1409. [PubMed: 24202393]

Malik SN, Brattain M, Ghosh PM, Troyer DA, Prihoda T, Bedolla R, and Kreisberg JI (2002). Immunohistochemical demonstration of phospho-Akt in high Gleason grade prostate cancer. Clin. Cancer Res 8, 1168–1171. [PubMed: 11948129]

Malonia SK, Dutta P, Santra MK, and Green MR (2015). F-box protein FBXO31 directs degradation of MDM2 to facilitate p53-mediated growth arrest following genotoxic stress. Proc. Natl. Acad. Sci. USA 112, 8632–8637. [PubMed: 26124108]

Manning BD, and Cantley LC (2007). AKT/PKB signaling: navigating downstream. Cell 129, 1261–1274. [PubMed: 17604717]

Manning BD, and Toker A (2017). AKT/PKB Signaling: Navigating the Network. Cell 169, 381–405. [PubMed: 28431241]

Marshall CJ (1995). Specificity of receptor tyrosine kinase signaling: transient versus sustained extracellular signal-regulated kinase activation. Cell 80, 179–185. [PubMed: 7834738]

Mendoza MC, Er EE, and Blenis J (2011). The Ras-ERK and PI3K-mTOR pathways: cross-talk and compensation. Trends Biochem. Sci 36, 320–328. [PubMed: 21531565]

Messina S, Frati L, Leonetti C, Zuchegna C, Di Zazzo E, Calogero A, and Porcellini A (2011). Dual-specificity phosphatase DUSP6 has tumor-promoting properties in human glioblastomas. Oncogene 30, 3813–3820. [PubMed: 21499306]

Molina G, Vogt A, Bakan A, Dai W, Queiroz de Oliveira P, Znosko W, Smithgall TE, Bahar I, Lazo JS, Day BW, and Tsang M (2009). Zebrafish chemical screening reveals an inhibitor of Dusp6 that expands cardiac cell lineages. Nat. Chem. Biol 5, 680–687. [PubMed: 19578332]

Moro L, Simoneschi D, Kurz E, Arbini AA, Jang S, Guaragnella N, Giannattasio S, Wang W, Chen YA, Pires G, et al. (2020). Epigenetic silencing of the ubiquitin ligase subunit FBXL7 impairs c-SRC degradation and promotes epithelial-to-mesenchymal transition and metastasis. Nat. Cell Biol 22, 1130–1142. [PubMed: 32839549]

Muda M, Boschert U, Dickinson R, Martinou JC, Martinou I, Camps M, Schlegel W, and Arkinstall S (1996). MKP-3, a novel cytosolic protein-tyrosine phosphatase that exemplifies a new class of mitogen-activated protein kinase phosphatase. J. Biol. Chem 271, 4319–4326. [PubMed: 8626780]

Oh E, Akopian D, and Rape M (2018). Principles of Ubiquitin-Dependent Signaling. Annu. Rev. Cell Dev. Biol 34, 137–162. [PubMed: 30110556]

Okudela K, Yazawa T, Woo T, Sakaeda M, Ishii J, Mitsui H, Shimoyamada H, Sato H, Tajiri M, Ogawa N, et al. (2009). Down-regulation of DUSP6 expression in lung cancer: its mechanism and potential role in carcinogenesis. Am. J. Pathol 175, 867–881. [PubMed: 19608870]

Paweletz CP, Charboneau L, Bichsel VE, Simone NL, Chen T, Gillespie JW, Emmert-Buck MR, Roth MJ, Petricoin EF III, and Liotta LA (2001). Reverse phase protein microarrays which capture disease progression show activation of pro-survival pathways at the cancer invasion front. Oncogene 20, 1981–1989. [PubMed: 11360182]

Petroski MD, and Deshaies RJ (2005). Function and regulation of cullin-RING ubiquitin ligases. Nat. Rev. Mol. Cell Biol 6, 9–20. [PubMed: 15688063]

Pickart CM (2004). Back to the future with ubiquitin. Cell 116, 181–190. [PubMed: 14744430]

Pratilas CA, Taylor BS, Ye Q, Viale A, Sander C, Solit DB, and Rosen N (2009). (V600E)BRAF is associated with disabled feedback inhibition of RAF-MEK signaling and elevated transcriptional output of the pathway. Proc. Natl. Acad. Sci. USA 106, 4519–4524. [PubMed: 19251651]

Ramkissoon A, Chaney KE, Milewski D, Williams KB, Williams RL, Choi K, Miller A, Kalin TV, Pressey JG, Szabo S, et al. (2019). Targeted Inhibition of the Dual Specificity Phosphatases DUSP1 and DUSP6 Suppress MPNST Growth via JNK. Clin. Cancer Res 25, 4117–4127. [PubMed: 30936125]

Ran FA, Hsu PD, Wright J, Agarwala V, Scott DA, and Zhang F (2013). Genome engineering using the CRISPR-Cas9 system. Nat. Protoc 8, 2281–2308. [PubMed: 24157548]

Rodriguez-Viciana P, Warne PH, Dhand R, Vanhaesebroeck B, Gout I, Fry MJ, Waterfield MD, and Downward J (1994). Phosphatidylinositol-3-OH kinase as a direct target of Ras. Nature 370, 527–532. [PubMed: 8052307]

Roskoski R Jr. (2012). ERK1/2 MAP kinases: structure, function, and regulation. Pharmacol. Res 66, 105–143. [PubMed: 22569528]

Santra MK, Wajapeyee N, and Green MR (2009). F-box protein FBXO31 mediates cyclin D1 degradation to induce G1 arrest after DNA damage. Nature 459, 722–725. [PubMed: 19412162]

Senft D, Qi J, and Ronai ZA (2018). Ubiquitin ligases in oncogenic transformation and cancer therapy. Nat. Rev. Cancer 18, 69–88. [PubMed: 29242641]

Shen MM, and Abate-Shen C (2010). Molecular genetics of prostate cancer: new prospects for old challenges. Genes Dev. 24, 1967–2000. [PubMed: 20844012]

Shojaee S, Caeser R, Buchner M, Park E, Swaminathan S, Hurtz C, Geng H, Chan LN, Klemm L, Hofmann WK, et al. (2015). Erk Negative Feedback Control Enables Pre-B Cell Transformation and Represents a Therapeutic Target in Acute Lymphoblastic Leukemia. Cancer Cell 28, 114–128. [PubMed: 26073130]

Simanshu DK, Nissley DV, and McCormick F (2017). RAS Proteins and Their Regulators in Human Disease. Cell 170, 17–33. [PubMed: 28666118]

Simoneschi D, Rona G, Zhou N, Jeong YT, Jiang S, Milletti G, Arbini AA, O'Sullivan A, Wang AA, Nithikasem S, et al. (2021). $CRL4^{AMBRA1}$ is a master regulator of D-type cyclins. Nature 592, 789–793. [PubMed: 33854235]

Skaar JR, and Pagano M (2009). Control of cell growth by the SCF and APC/C ubiquitin ligases. Curr. Opin. Cell Biol 21, 816–824. [PubMed: 19775879]

Skaar JR, D'Angiolella V, Pagan JK, and Pagano M (2009). SnapShot: F Box Proteins II. Cell 137, 1358.e1351. [PubMed: 19563764]

Skaar JR, Pagan JK, and Pagano M (2013). Mechanisms and function of substrate recruitment by F-box proteins. Nat. Rev. Mol. Cell Biol 14,369–381. [PubMed: 23657496]

Skaar JR, Pagan JK, and Pagano M (2014). SCF ubiquitin ligase-targeted therapies. Nat. Rev. Drug Discov 13, 889–903. [PubMed: 25394868]

Tan Y, Liu D, Gong J, Liu J, and Huo J (2018). The role of F-box only protein 31 in cancer. Oncol. Lett 15, 4047–4052. [PubMed: 29556284]

Taylor BS, Schultz N, Hieronymus H, Gopalan A, Xiao Y, Carver BS, Arora VK, Kaushik P, Cerami E, Reva B, et al. (2010). Integrative genomic profiling of human prostate cancer. Cancer Cell 18, 11–22. [PubMed: 20579941]

Turke AB, Song Y, Costa C, Cook R, Arteaga CL, Asara JM, and Engelman JA (2012). MEK inhibition leads to PI3K/AKT activation by relieving a negative feedback on ERBB receptors. Cancer Res. 72, 3228–3237. [PubMed: 22552284]

Unni AM, Harbourne B, Oh MH, Wild S, Ferrarone JR, Lockwood WW, and Varmus H (2018). Hyperactivation of ERK by multiple mechanisms is toxic to RTK-RAS mutation-driven lung adenocarcinoma cells. eLife 7, e33718. [PubMed: 30475204]

von Kriegsheim A, Baiocchi D, Birtwistle M, Sumpton D, Bienvenut W, Morrice N, Yamada K, Lamond A, Kalna G, Orton R, et al. (2009). Cell fate decisions are specified by the dynamic ERK interactome. Nat. Cell Biol 11, 1458–1464. [PubMed: 19935650]

Wang Z, Liu P, Inuzuka H, and Wei W (2014). Roles of F-box proteins in cancer. Nat. Rev. Cancer 14, 233–247. [PubMed: 24658274]

Wang G, Zhao D, Spring DJ, and DePinho RA (2018). Genetics and biology of prostate cancer. Genes Dev. 32, 1105–1140. [PubMed: 30181359]

Webber MM, Quader STA, Kleinman HK, Bello-DeOcampo D, Storto PD, Bice G, DeMendonca-Calaca W, and Williams DE (2001). Human cell lines as an in vitro/in vivo model for prostate carcinogenesis and progression. Prostate 47, 1–13. [PubMed: 11304724]

Wu QN, Liao YF, Lu YX, Wang Y, Lu JH, Zeng ZL, Huang QT, Sheng H, Yun JP, Xie D, et al. (2018). Pharmacological inhibition of DUSP6 suppresses gastric cancer growth and metastasis and overcomes cisplatin resistance. Cancer Lett. 412, 243–255. [PubMed: 29050982]

Yu CF, Liu ZX, and Cantley LG (2002). ERK negatively regulates the epidermal growth factor-mediated interaction of Gab1 and the phosphatidylinositol 3-kinase. J. Biol. Chem 277, 19382–19388. [PubMed: 11896055]

Zhang Z, Kobayashi S, Borczuk AC, Leidner RS, Laframboise T, Levine AD, and Halmos B (2010). Dual specificity phosphatase 6 (DUSP6) is an ETS-regulated negative feedback mediator of oncogenic ERK signaling in lung cancer cells. Carcinogenesis 31, 577–586. [PubMed: 20097731]

Highlights

- $CRL1^{FBXO31}$ induces the ubiquitin-mediated degradation of DUSP6
- DUSP6 stabilization suppresses ERK signaling and activates PI3K-AKT signaling
- FBXO31 acts as a tumor suppressor in prostate cancer
- Inhibition of DUSP6 with BCI prevents prostate tumor formation

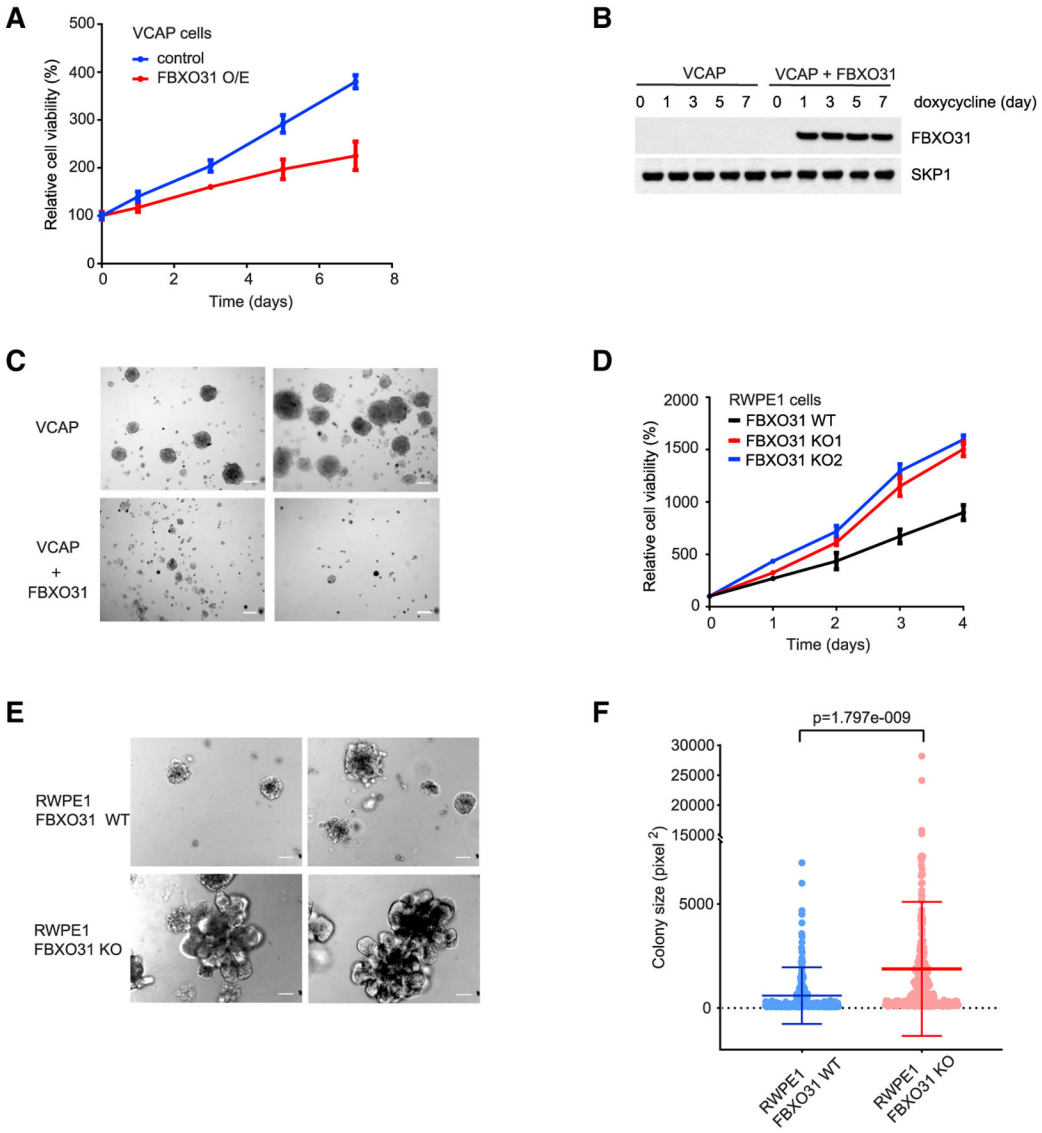

Figure 1. Deletion of *FBXO31* promotes prostate cell growth

(A) VCAP cells were transduced with a doxycycline-inducible vector system for mthe expression of FBXO31. Cells expressing doxycycline-inducible FBXO31 or empty vector (EV) were plated and treated with doxycycline for the indicated times. The relative cell growth was then measured by ATP-Glo assay. Growth curves were generated with Prism 8 (mean ± SD; n = 8).

(B) The expression levels of FBXO31 in the experiments shown in (A) were examined by western blotting. SKP1 was used as a control.

(C) Representative images of control VCAP cells and cells with induced FBXO31 expression in 3D culture (scale bar: 100 uM).

(D) *FBXO31* wild-type or knockout (KO) RWPE1 cells were plated and cultured for the indicated days. Cell growth was then determined by ATP-Glo assay. Graph was generated using Prism 8 (mean ± SD; n = 8).

(E) Parental and *FBXO31* KO RWPE1 cells were put into 3D culture. Representative pictures of cells grown in 3D culture are shown (scale bar: 100 uM).
(F) Colony sizes of parental or *FBXO31* KO RWPE1 cells grown in 3D culture were measured and analyzed using ImageJ. The dots and error bars represent the mean ± SD values.

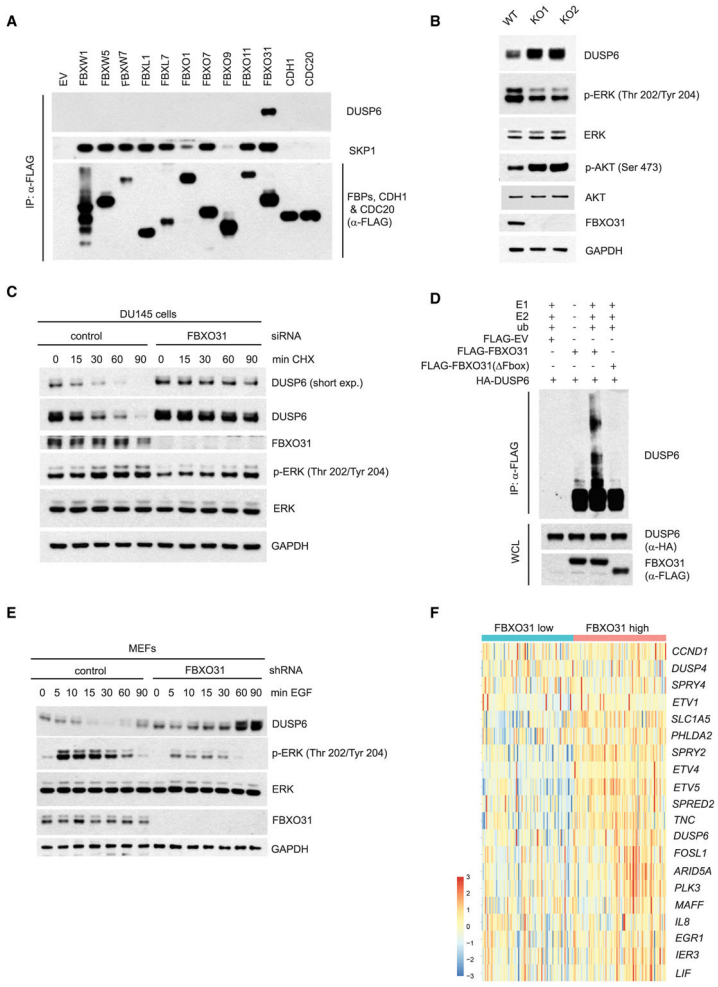

Figure 2. FBXO31 mediates DUSP6 degradation and regulates ERK signaling

(A) 293H cells were transfected with plasmids expressing the indicated proteins. Cells were treated with the proteasome inhibitor MG132 for 4 h. Cell lysates were then immunoprecipitated with an anti-FLAG resin, and the immunoprecipitates were probed with the indicated antibodies.

(B) Parental RWPE1 cells and two *FBXO31* KO RWPE1 clones were subjected to western blot analysis using the indicated antibodies.

(C) DU145 cells were transfected with either non-targeting control siRNA or siRNA against *FBXO31*. Cells were then treated with cycloheximide (CHX) for the indicated times. Protein extracts were immunoblotted for the indicated proteins.

(D) 293H cells were transfected with hemagglutinin (HA)-tagged DUSP6, FLAG-tagged FBXO31, or its F-box domain deletion mutant (ΔFbox) as indicated. After immunopurification (IP) with anti-FLAG resin, *in vitro* ubiquitylation of DUSP6 was performed in the presence or absence of E1, E2s (UbcH3 and ubcH5), and ubiquitin (ub). Samples were analyzed by immunoblotting with an anti-DUSP6 antibody. Immunoblots of whole-cell lysates (WCLs) are shown at the bottom.

(E) MEFs stably expressing a control shRNA or a shRNA against *FBXO31* were serum-starved overnight, then stimulated with EGF (100 ng/mL). Samples were collected at the indicated time points for immunoblotting analysis.

(F) The expression levels of ERK signaling-regulated genes in prostate patient samples with higher (top 25%) or lower (bottom 25%) FBXO31 mRNA levels are depicted as a heatmap. RNA sequencing (RNA-seq) data were obtained from the TCGA dataset of human prostate adenocarcinoma (Cancer Genome Atlas Research Network, 2015).

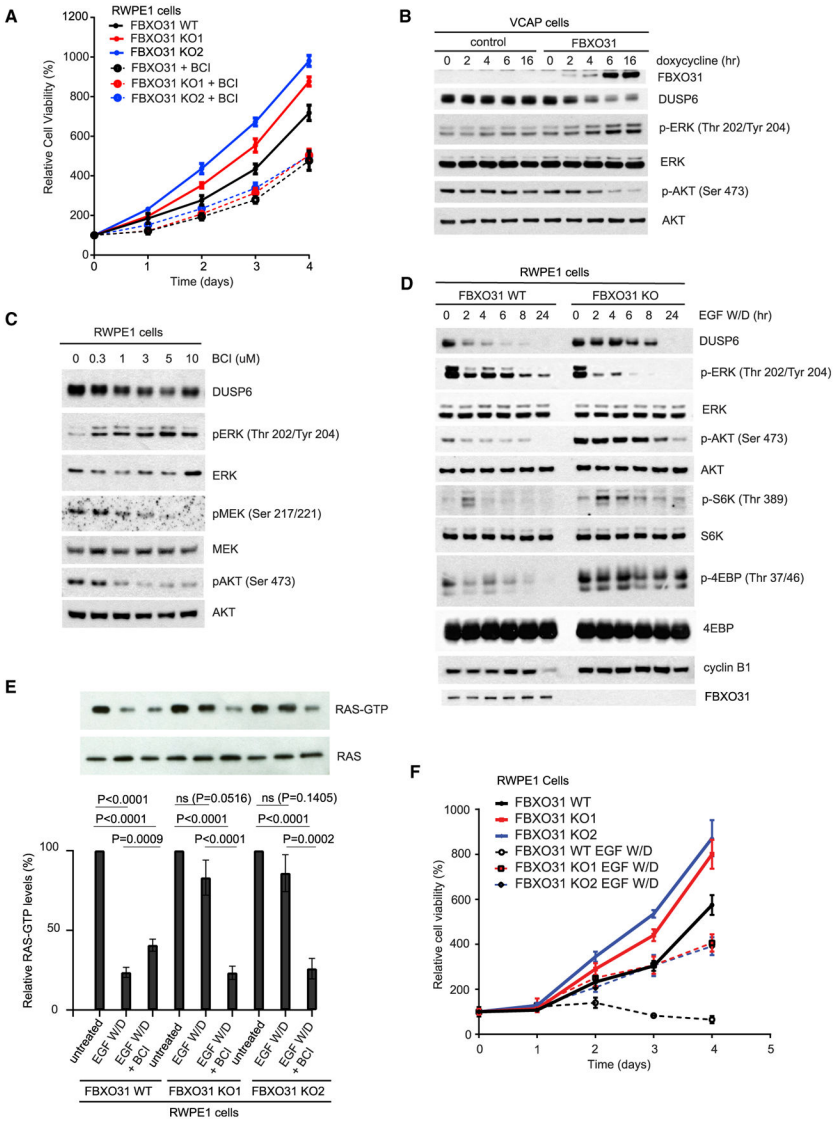

Figure 3. Depletion of FBXO31 regulates ERK and AKT activity and promotes cell growth in prostate cells

(A) Parental and *FBXO31* KO RWPE1 cells were treated with vehicle or the DUSP6 inhibitor BCI for the indicated days, and cell viability was determined by ATP-Glo assay. Graph was generated using Prism 8 (mean ± SD; n = 8).

(B) VCAP cells stably transduced with a retroviral system expressing doxycycline-inducible FBXO31 or a control vector were treated with doxycycline for the indicated times. WCLs were immunoblotted as indicated.

(C) RWPE1 cells were treated with various concentrations of BCI for 6 h and then analyzed by immunoblotting for the indicated proteins.

(D) *FBXO31* wild-type or KO RWPE1 cells were cultured in medium without EGF for the indicated times (withdrawal [W/D]) and then harvested and analyzed by immunoblotting.

(E) *FBXO31* wild-type or KO RWPE1 cells were cultured in regular medium or in medium without EGF (W/D). Where indicated, cells were treated with the DUSP6 inhibitor BCI. GTP-bound RAS was quantified using RAF1 Ras-binding domain (RBD) pull-down assay.

Western blotting images are representative of 3 independent experiments, and the intensity of bands was quantified by ImageJ. The columns represent the relative levels of RAS-GTP as normalized to the levels of total RAS protein (mean ± SD; n = 3 independent experiments)

(F) *FBXO31* wild-type or KO RWPE1 cells were cultured in regular medium or medium without EGF. Relative cell viability was measured by ATP-Glo assay. Graph was generated using Prism 8 (mean ± SD; n = 8).

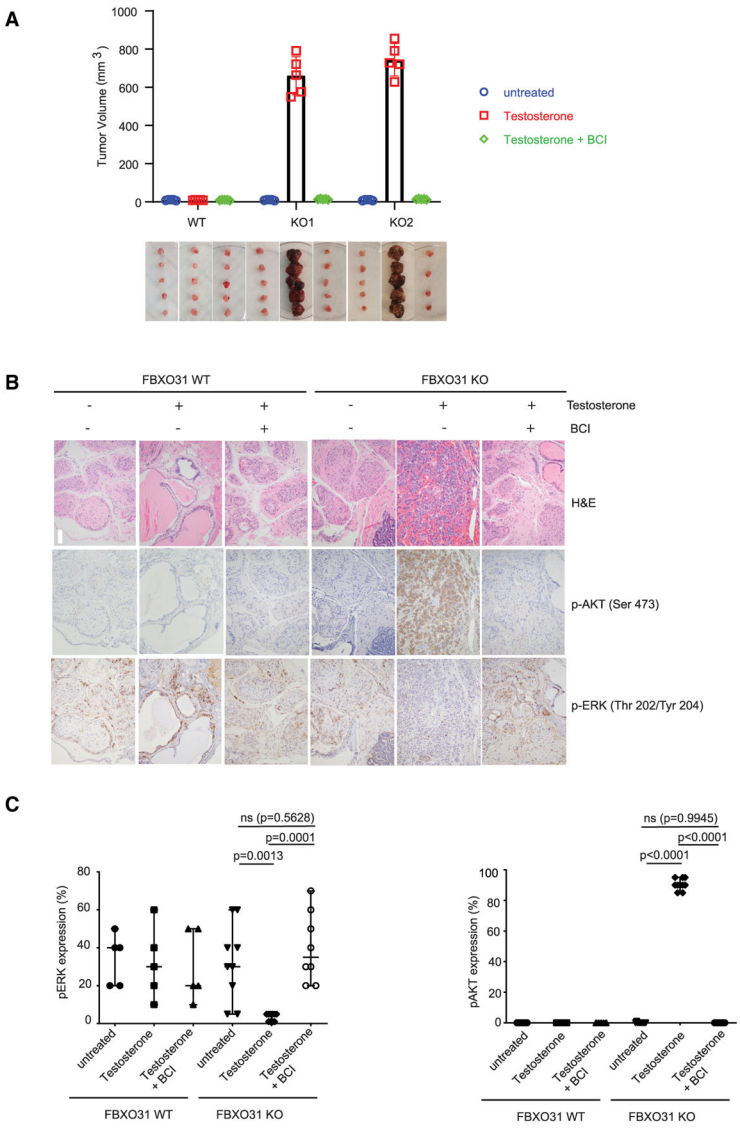

Figure 4. Loss of *FBXO31* promotes tumor growth in mouse prostate

(A) *FBXO31* wild-type or KO RWPE1 cells were injected into NSG (NOD scid gamma) mice (n = 5 for each group) in the absence or presence of testosterone. Mice were treated with vehicle (PBS) or the DUSP6 inhibitor BCI. Orthotopic tumors formed from *FBXO31* KO RWPE1 cells were dissected. The volume of the dissected tumors was then measured. Graph was generated using Prism 8 (mean ± SD).

(B) Representative histology in the orthotopic xenografts described in (A) stained with H&E and with antibodies against p-ERK or p-AKT (scale bar: 1 mm).

(C) Quantification of p-ERK or p-AKT positive staining in orthotopic xenografts using *FBXO31* KO RWPE1 cells and parental RWPE1 cells (untreated, n = 10; testosterone, n = 10; testosterone + BCI treatment, n = 9). Graph was generated using Prism 8 (mean ± SD).

KEY RESOURCES TABLE

REAGENT or RESOURCE	SOURCE	IDENTIFIER
Antibodies		
anti-FBXO31	Novus	Cat. No. NBP1-19088, RRID:AB_1642033
Anti-FBXO31	Bethyl Laboratories	Cat. No. A302-047A, RRID:AB_1604217
anti-DUSP6	Abcam	Cat. No. ab76310, RRID:AB_1523517
anti-p44/42 MAPK (ERK1/2)	Cell Signaling Technology	Cat. No. 9107, RRID:AB_10695739
anti-p-p44/42 MAPK (T202/Y204)	Cell Signaling Technology	Cat. No. 4370, RRID:AB_2315112
anti-p-AKT S473	Cell Signaling Technology	Cat. No. 4058, RRID:AB_331168
anti-AKT (clone 9Q7)	Thermo Fisher Scientific	Cat. No. AHO1112, RRID:AB_2536322
anti-p-AKT S473	Cell Signaling Technology	Cat. No. 4060, RRID:AB_2315049
anti-p-p70 S6 kinase (T389)	Cell Signaling Technology	Cat. No. 9206, RRID:AB_2285392
anti-p70 S6 kinase	Cell Signaling Technology	Cat. No. 2708, RRID:AB_390722
anti-MEK1	Cell Signaling Technology	Cat. No. 2352, RRID:AB_10693788
anti-p-MEK1/2	Cell Signaling Technology	Cat. No. 9154, RRID:AB_2138017
anti-p-S6 (S235/236)	Cell Signaling Technology	Cat. No. 4858, RRID:AB_916156
anti-p-4E-BP1 (Thr37/46)	Cell Signaling Technology	Cat. No. 2855, RRID:AB_560835
anti-p-4E-BP1 (Ser65)	Cell Signaling Technology	Cat. No. 9456, RRID:AB_823413
anti-4E-BP1	Cell Signaling Technology	Cat. No. 9452, RRID:AB_331692
anti-CUL1	Thermo Fisher Scientific	Cat. No. 322400, RRID:AB_2533070
anti-GAPDH	Cell Signaling Technology	Cat. No. 97166, RRID:AB_2756824
anti-FLAG (M2)	Sigma-Aldrich	Cat. No. F1804, RRID:AB_262044
anti-FLAG	Sigma-Aldrich	Cat. No. F7425, RRID:AB_439687
anti-FLAG (M2) Affinity Gel	Sigma-Aldrich	Cat. No. A2220, RRID:AB_10063035
anti-HA	Biolegend	Cat. No. 901503, RRID:AB_2565005
anti-HA Affinity Matrix	Roche	Cat. No. 11815016001, RRID:AB_390914
anti-SKP1	Santa Cruz Biotechnology	Cat. No. sc-5281, RRID:AB_2254579
anti-ubiquitin	Millipore	Cat. No. 04-263, RRID:AB_612093
Bacterial and virus strains		
NEB5-*alpha*	Promega	Cat. No. C2992H
Chemicals, peptides, and recombinant proteins		
Doxycycline (0.1 μg/mL)	Sigma-Aldrich	Cat. No. D9891
Lipofectamine 3000	Invitrogen	Cat. No. L3000150
Lipofectamine RNAi Max	Invitrogen	Cat No. 13778-500
MG132 (10 μM)	Peptides International	Cat. No. IZL-3175v
MLN4924 (2 μM)	Active Biochem	Cat. No. A-1139
Polybrene (8 mg/mL)	Sigma-Aldrich	Cat. No. TR-1003
Puromycin (1 μg/mL)	Sigma-Aldrich	Cat. No. P9620
Cycloheximide (50 μg/mL)	Sigma-Aldrich	Cat. No. C7698-1G
(E/Z)-BCI hydrochloride	Sigma-Aldrich	Cat. No. B4313
PhosSTOP	Sigma-Aldrich	Cat. No. 4906837001
cOmplete(TM) ULTRA Tablets	Sigma-Aldrich	Cat. No. 5892953001

REAGENT or RESOURCE	SOURCE	IDENTIFIER
Matrigel Matrix Phenol Red-Free	Corning	Cat. No. 356237
Recombinant Human EGF Protein	R&D Systems	Cat. No. 236-EG-200
Recombinant human ubiquitin activating enzyme (UBE1)	Boston Biochem	E-305
Recombinant Human His6-UBE2R1/CDC34 Protein	Boston Biochem	E2-610
Recombinant Human UbcH5c/UBE2D3 Protein	Boston Biochem	E2-627
Recombinant Human Ubiquitin Protein	Boston Biochem	U-100H
Recombinant Human Ubiquitin Aldehyde Protein	Boston Biochem	U-201
Critical commercial assays		
CellTiter-Glo® Luminescent Cell Viability Assay	Promega	Cat. No. G7570
CellTiter-Glo® 3D Cell Viability Assay	Promega	Cat. No. G9681
RNA to cDNA EcoDry™ Premix (Oligo dT)	Clontech	Cat. No. 639543
Deposited data		
Original images of western blot data	This study; Mendeley Data	https://doi.org/10.17632/m5r6nk52tg.1
Experimental models: Cell lines		
HEK293T	ATCC	Cat. No. CRL-3216
293H	Thermo Fisher Scientific	Cat. No. 11631017
VCAP	ATCC	Cat. No. CRL-2876
A375	ATCC	Cat. No. CRL-1619
SK-MEL-28	ATCC	Cat. No. HTB-72
MEFs	Michele Pagano Laboratory	N/A
RWPE1	ATCC	Cat. No. CRL-11609
Experimental models: Organisms/strains		
NSG (NOD.Cg-*Prkdc*^{scid} *Il2rg*^{tm1Wjl}/SzJ)	Jackson Laboratory	Cat. No 005557
Oligonucleotides		
hFBXO31_gRNA#1 forward	Integrated DNA Technologies	5′-caccgGCGACGGGCCCACGCCGCAA-3′
hFBXO31_gRNA#1 reverse	Integrated DNA Technologies	5′-aaacTTGCGGCGTGGGCCCGTCGCc-3′
hFBXO31_gRNA#2 forward	Integrated DNA Technologies	5′-caccgGGCGCCGACATCCGCGCGAC-3′
hFBXO31_gRNA#2 reverse	Integrated DNA Technologies	5′-aaacGTCGCGCGGATGTCGGCGCCc-3′
CRISPR genotyping forward	Integrated DNA Technologies	5′-GTTTTGCACTCGGCATCAC-3′
CRISPR genotyping reverse	Integrated DNA Technologies	5′-CCCTAACCGCCTCAAATACC-3′
Recombinant DNA		
pSpCas9(BB)-2A-GFP (PX458)	Addgene	Cat. No. 48138
TTIGp-MLUEX-FBXO31	Michele Pagano Laboratory	N/A
TTIGp-MLUEX	Neal Rosen's laboratory, MSKCC, NYC	N/A
pMSCV-rtTA3	Neal Rosen's laboratory, MSKCC, NYC	N/A
p3XFLAG-CMV	Sigma-Aldrich	E9283
p3XFLAG-CMV-FBXO31	Michele Pagano Laboratory	N/A
p3XFLAG-CMV-FLAG-FBXO31(ΔFbox)	Michele Pagano Laboratory	N/A
pCMV-Tag2B-HA-DUSP6	Michele Pagano Laboratory	N/A

REAGENT or RESOURCE	SOURCE	IDENTIFIER
pCMV-Tag2B-HA-DUSP61-154	Michele Pagano Laboratory	N/A
pCMV-Tag2B-HA-DUSP6 1-204	Michele Pagano Laboratory	N/A
pCMV-Tag2B-HA-DUSP6 1-347	Michele Pagano Laboratory	N/A
pCMV-Tag2B-HA-DUSP6 154-381	Michele Pagano Laboratory	N/A
pCMV-Tag2B-HA-DUSP6 31-381	Michele Pagano Laboratory	N/A
pCMV-Tag2B-HA-DUSP6 60-381	Michele Pagano Laboratory	N/A
pCMV-Tag2B-HA-DUSP6 91-381	Michele Pagano Laboratory	N/A
pCMV-Tag2B-HA-DUSP6 Δ 154-203	Michele Pagano Laboratory	N/A
pCMV-Tag2B-HA-DUSP6 Δ 92-154	Michele Pagano Laboratory	N/A
pCMV-Tag2B-HA-DUSP6 Δ 92-125	Michele Pagano Laboratory	N/A
pCMV-Tag2B-HA-DUSP6 Δ 126-137	Michele Pagano Laboratory	N/A
pCMV-Tag2B-HA-DUSP6 Δ 137-154	Michele Pagano Laboratory	N/A
Software and algorithms		
GraphPad Prism 8	GraphPad Software	https://www.graphpad.com/scientific-software/prism/
Slidepath software version 4.0.8	Leica Microsystems	N/A